Organic & Biomolecular Chemistry

Accepted Manuscript

This article can be cited before page numbers have been issued, to do this please use: B. Han, C. Peng, B. Wang, W. Huang, J. Zhou, X. Tang and Y. Chen, *Org. Biomol. Chem.*, 2017, DOI: 10.1039/C7OB01429E.

ROYAL SOCIETY OF CHEMISTRY

rsc.li/obc

View Article Online
DOI: 10.1039/C7OB01429E

Organic & Biomolecular Chemistry

ARTICLE

Drug design based on pentaerythritol tetranitrate reductase: synthesis and antibacterial activity of Pogostone derivatives†

Received 00th January 20xx,
Accepted 00th January 20xx

DOI: 10.1039/x0xx00000x

www.rsc.org/

Biao Wang,‡[a] Wei Huang,‡[b] Jin Zhou,[a] Xue Tang,[a] Yang Chen,[b] Cheng Peng*[ab] and Bo Han*[a]

Our previous work showed that Pogostone exerts antibacterial effects by targeting pentaerythritol tetranitrate reductase (PETNR). In order to develop derivatives of Pogostone with potent antibacterial activity, we performed molecular docking studies of Pogostone with PETNR and analyzed structure-activity relationships, which guided the structure design and the subsequent facile organocatalytic synthesis of Pogostone derivatives under mild reaction conditions. Several of the synthesized compounds showed antibacterial activity *in vitro*, including one compound (**3h**) that was highly effective against methicillin-resistant *Staphylococcus aureus*. These results suggest that Pogostone derivatives bearing functional groups on the side chain may be good leads for antibacterial drug development.

Introduction

While antibiotics have revolutionized the treatment of bacterial infections,[1] the abundant use of certain types such as β-lactams, macrolides, and tetracyclines, has contributed to the emergence of resistant strains and made it difficult to determine the most effective antibiotic for a given infection.[2] This has led to an explosion of interest in designing and synthesizing novel drugs that can treat bacteria already resistant to existing drugs.[3,4]

Natural products have served for a long time as the inspiration for drug design, particularly against infectious diseases.[5] Natural products often feature molecular scaffolds and pharmacophore motifs that confer desirable biological activities.[6] Modification of the core structure of natural products can improve their physical and chemical properties, enhance their biological activity, reduce toxicity, and bypass drug resistance pathways in the host.[7] Using this approach, for example, the Hergenrother group reported a deoxynybomycin-inspired, fragment-like lead compound with potent activity against *Staphylococcus aureus* (*S. aureus*) and greater aqueous solubility than the parent compound.[8] Our goal is therefore to draw from natural products to guide the design of novel antibacterials, particularly against resistant bacteria.

We focused on Pogostone, one of the main compounds in patchouli volatile oil, which is isolated from the Chinese herb *Pogostemon cablin* and which exerts a variety of biological activities, including regulation of gastrointestinal function, inhibition of inflammation and inhibition of bacterial growth.[9] Pogostone inhibits growth of *Candida albicans*, *Cryptococcus neoformans*, *Rhizopus nigricans* and other fungi,[10] as well as *Escherichia coli* (*E. coli*) and methicillin-resistant *Staphylococcus aureus* (MRSA).[11] The Pogostone monomer shows a minimum inhibitory concentration (MIC) < 0.098 μg/ml against *Chryseobacterium indologenes* and *Corynebacterium xerosis*,[11] and pharmacokinetic studies indicate good oral absorption.[12] Our previous work has identified one of the targets of Pogostone to be pentaerythritol tetranitrate reductase (PETNR, Uniprot P71278),[13] an NAD(P)H- and FMN-dependent oxidoreductase with a key role in nitrogen fixation and therefore in bacterial growth and metabolism.[14] Bacteria can be inhibited by PETNR-targeting antimicrobials, and the bactericidal mechanisms of these chemical substances differ from the mechanisms of traditional antibiotics. All these factors make Pogostone highly attractive for derivatization aimed at generating novel drug leads that may overcome host resistance to traditional antibiotics.

Results and discussion

We performed molecular docking studies of Pogostone with PETNR in order to analyze structure-activity relationships, which we used to guide facile synthetic derivatization. Docking studies suggest that the core moiety of dehydroacetic acid (DHA)[15] interacts with the protein via hydrogen bonding, van der Waals forces, and electrostatic forces (Fig. 1a-b). In addition, a strong intermolecular π-π interaction may form between DHA and the FMN coenzyme of PETNR (Fig 1c). We observed a large

[a] State Key Laboratory Breeding Base of Systematic Research, Development and Utilization of Chinese Medicine Resources, Chengdu University of Traditional Chinese Medicine, Chengdu 611137, China. E-mail: hanbo@cdutcm.edu.cn
[b] Ministry of Education Key Laboratory of Standardization of Chinese Medicine, School of Pharmacy, Chengdu University of Traditional Chinese Medicine, Chengdu 611137, China. E-mail: pengcheng@cdutcm.edu.cn

† Electronic supplementary information (ESI) available: Experimental procedures and characterization data for new compounds. CCDC 1555526. For ESI and crystallographic data in CIF or other electronic format see DOI: 10.1039/x0xx00000x
‡ These authors contributed equally to this work.

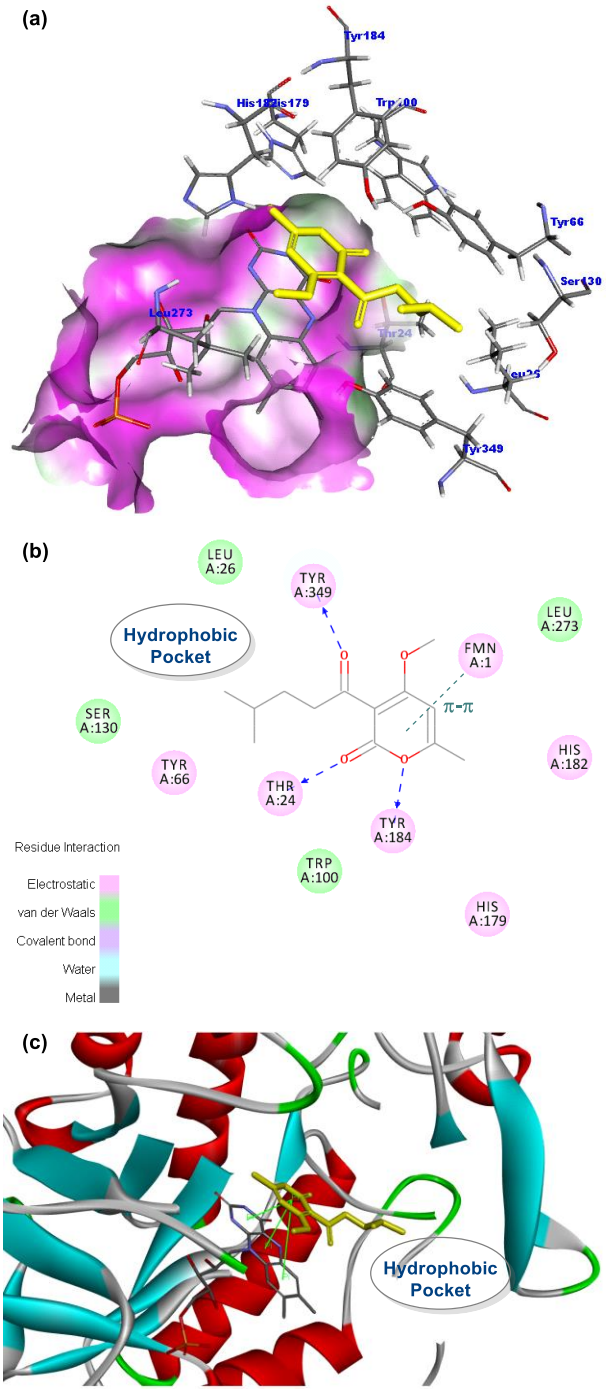

Fig. 1 Molecular docking of Pogostone (ball-and-stick) and PETNR (space-filling). The hydrophobic binding pocket in PETNR and the Pogostone moiety targeted for derivatization are shown. (a) 3D binding mode of Pogostone with key amino acid residues of PETNR. The binding pocket is shaped through H-bond interactions. (b) 2D contour of the binding mode generated using the Accelrys Discovery Studio Package, including electrostatic interactions (pink), van der Waals forces (green) and H-bond interactions (blue arrow). (c) π-π interaction between DHA and the FMN coenzyme.

hydrophobic cavity around the side chain of Pogostone (Fig. 1b-c), and we reasoned that introducing a sterically hindered hydrophobic group at the side chain may improve Pogostone binding to the protein. Consistent with this idea, adding functional group with saturated aldehyde to the side chain of Pogostone moderately enhances its antibacterial activity.[16] Therefore we aimed to develop an efficient method to generate Pogostone derivatives with diverse substitutions on the side chain, which we would evaluate against pathogenic bacteria as well as antibiotic-resistant bacteria. In addition to filling the hydrophobic cavity, the substitutions on the side chain may improve antibacterial activity through steric and electronic effects. We envisaged that the results would help the work of our own group and others to develop efficient and convenient reactions to assemble synthetically important scaffolds as potential drug leads.[17]

We planned to use organocatalysis[18] to modify the side chain of Pogostone with an α,β-unsaturated aldehyde (Scheme 1), which contrasts with the published "saturated aldehyde-strategy".[16] We knew that the terminal methyl group on the Pogostone core would be much less reactive than methylene in the planned Knoevenagel condensation, and we knew that we could not entirely avoid the side reaction of Michael addition. Nevertheless, we speculated that we could make the desired Knoevenagel condensation more favorable by reducing the LUMO energy of the unsaturated aldehyde *via* iminium catalysis.

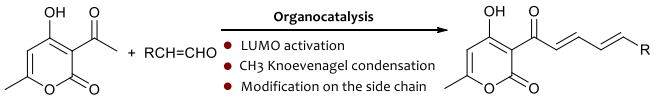

Scheme 1 Synthetic strategy.

We began our studies by exploring the model reaction of DHA **1** (0.3 mmol) with cinnamyl aldehyde **2a** (0.36 mmol) in toluene at room temperature using pyrrolidine **C1** (0.06 mmol) as catalyst and benzoic acid as additive. To our gratification, the reaction proceeded smoothly to afford the desired compound **3a** in 52% yield, but with a double-Michael addition by-product **4a** (Table 1, entry 1). The *E* configuration of two conjugate alkenyl groups in the products was confirmed based on NMR coupling constants and X-ray crystallographic data (Fig. 2).[19] The *Z* isomer was not observed. Encouraged by these results, we optimized reaction conditions (Table 1). Using L-proline **C2** as catalyst led to much lower yield not only of condensation product but also of Michael addition by-product (entry 2). Using α,α-diphenylprolinol trimethylsilyl ether **C3** as catalyst afforded compound **3a** in 68% yield with both good catalytic activity and chemoselectivity (entry 3). We obtained higher yield when using bulkier silyl ethers **C4** and **C5** (entries 4 and 5), so we selected **C5** as the optimal catalyst. Solvent affected reaction efficiency to some extent (entries 6-9), with acetonitrile proving to be the best choice (entry 9). Screening other acid additives led to slightly lower yield (entries 10-11). Raising the reaction temperature to 60 °C did not improve reaction efficiency or yield of product **3a**, since the higher temperature promoted formation of the Michael addition by-product (entry 12). In the end, we defined the optimal reaction conditions as room temperature in the presence of catalyst **C5** at 20 mol%, benzoic acid as additive, and MeCN as solvent (entry 9).

Table 1 Optimization of reaction conditions[a]

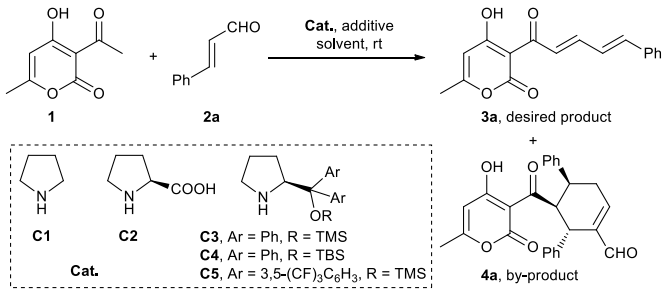

Entry	Cat.	Additive	Solvent	Yield of **3a**[b] (%)	Yield of **4a**[c] (%)
1	**C1**	BzOH	Toluene	52	15
2	**C2**	BzOH	Toluene	36	10
3	**C3**	BzOH	Toluene	68	<5
4	**C4**	BzOH	Toluene	72	<5
5	**C5**	BzOH	Toluene	78	<5
6	**C5**	BzOH	THF	74	<5
7	**C5**	BzOH	DCM	80	<5
8	**C5**	BzOH	Dioxane	74	<5
9	**C5**	BzOH	MeCN	86	<5
10	**C5**	AcOH	MeCN	80	<5
11	**C5**	*p*-F-BzOH	MeCN	79	<5
12[d]	**C5**	BzOH	MeCN	58	19

[a] Unless noted otherwise, reactions were performed with **1** (0.3 mmol), **2a** (0.36 mmol), **Cat.** (0.06 mmol) and acidic additive (0.12 mmol) in 2 mL solvent at rt. [b] Yield of isolated **3a**. [c] Yield of isolated **4a**. [d] The reaction was performed at 60 °C for 12h. Bz = benzoyl, TBS = *tert*-butyldimethylsilyl, TMS = trimethylsilyl.

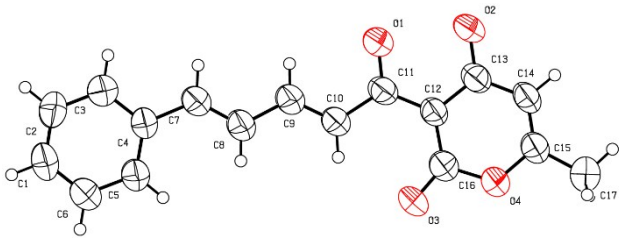

Fig. 2 ORTEP drawing of compound **3a**.

Using these optimal conditions, we explored the generality of this Pogostone derivatization reaction (Table 2). The reaction tolerated various substituents on the unsaturated aldehyde **2,** smoothly affording the corresponding products in 43-85% yield (entries 2-15). Unsaturated aromatic aldehydes **2b**-**2i**, which have electron-deficient substituents at the *ortho*, *meta* or *para* positions, gave higher yields in the condensation reaction than **2j**-**2l**, which have electron-rich substituents (entries 2-9 *vs* 10-12). The aromatic aldehyde **2c** with Cl at the *ortho* position gave the desired product **3c** in lower yield than the aldehydes

Table 2 Synthesis of Pogostone derivatives[a]

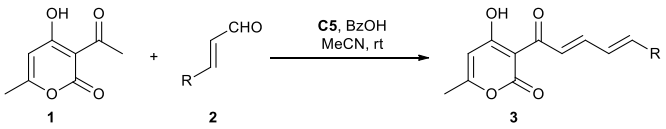

Entry	R	Product	Yield[b] (%)	*E*/*Z*[c]
1	C_6H_5	**3a**	86	>20:1
2	2-FC_6H_4	**3b**	81	>20:1
3	2-ClC_6H_4	**3c**	79	>20:1
4	2-$NO_2C_6H_4$	**3d**	80	>20:1
5	3-FC_6H_4	**3e**	82	>20:1
6	3-ClC_6H_4	**3f**	81	>20:1
7	4-FC_6H_4	**3g**	84	>20:1
8	4-ClC_6H_4	**3h**	87	>20:1
9	4-BrC_6H_4	**3i**	85	>20:1
10	4-MeC_6H_4	**3j**	75	>20:1
11	2-$OMeC_6H_4$	**3k**	75	>20:1
12	4-$OMeC_6H_4$	**3l**	77	>20:1
13	2-Furyl	**3m**	73	>20:1
14	$(CH_3)_2CH$	**3n**	49	>20:1
15	CH_3	**3o**	44	2.5:1

[a] Unless noted otherwise, reactions were performed with **1** (0.3 mmol), **2** (0.36 mmol), **C5** (0.06 mmol) and BzOH (0.12 mmol) in 2 mL acetonitrile at rt. [b] Yield of isolated **3**. [c] Determined by ^{1}H NMR analysis.

2f or **2h** with Cl at the *meta* or *para* position (entry 3 *vs* 6 and 8). These results suggest that the electron-donating conjugative effect may render substrate **2c** less electrophilic. The reaction tolerated heteroaromatic and aliphatic enals, such as 3-furanyl acrylaldehyde, butenal or 4-methyl-2-pentenal, generating the corresponding products in respective yields of 71%, 48%, and 43% (entries 13-15). In contrast to the high selectivity for the *Z* configuration in products **3a**-**3n** (>20:1), product **3o** showed more modest *Z* selectivity of 2.5:1 based on ^{1}H-NMR (entry 15).

With Pogostone derivatives **3a**-**3o** in hand, we screened them *in vitro* for antibacterial activity against six strains: *E. coli*, ATCC 25922 and CMCC 44102; *S. aureus*, ATCC 25923 and CMCC 26003; and MRSA, ATCC 43300 and 33591. Most derivatives proved inactive against Gram-negative *E. coli* (Table 3). In contrast, several Pogostone derivatives displayed promising antibacterial activity against Gram-positive *S. aureus* and MRSA. Compound **3h** showed the strongest activity against MRSA with a MIC of 8 μg/mL, comparable to the MIC of 4 and 1 μg/mL for the positive control antibiotics levofloxacin hydrochloride and vancomycin.[20] The screening results indicated that, in most cases, Pogostone derivatives bearing electron-deficient substituents showed stronger antibacterial activity (**3b**-**3i**) than derivatives bearing electron-rich substituents (**3j**-**3l**; MICs >256

to 512 μg/mL), heteroaromatic groups (**3m**; MICs >256 μg/mL) or alkyl groups (**3n** and **3o**; MICs 128 and 64 μg/mL). Among electron-deficient substituents, halogens were associated with more potent activity than nitro groups, with chlorine substituents giving optimal results. The position of the Cl substituent influenced antibacterial activity: *para*-Cl was associated with lower MIC (8 μg/mL) than *ortho*-Cl (128 μg/mL) or *meta*-Cl (128 μg/mL). These results identify compound **3h** as potently inhibiting Gram-positive bacterial strains, especially MRSA, at relatively low concentrations. This compound may be a promising lead for developing novel antibacterial agents that can bypass resistance.

Next, we performed molecular docking studies to generate the bioactive binding poses of Pogostone derivatives in the active site of PETNR by using the LibDock module in DS software. The LibDock scores were presented in the Table 3. The trend of the LibDock scores were basically consentient with the antibacterial activities.

The derivative **3h** with the highest docking score and antibacterial activity was selected for further investigation, and its interaction pattern with the binding site are shown in Figure 3a. A 2D diagram (Figure 3b) showing various interactions, such as hydrogen bonds, van der Waals forces, electrostatic forces, and π-π interaction between compound **3h** and the FMN coenzyme of PETNR was also presented. We also parallelly compared the docked binding modes (Figure 3c) of both Pogostone (yellow skeleton) and optimized compound **3h** (blue skeleton). Importantly, the large hydrophobic cavity previously observed around the side chain of Pogostone core has been occupied by the conjugate functional group (Figure 3a-c), and the newly introduced double bond and *para*-Cl substituent on the aromatic ring played an important role in the ligand-protein interaction.

Moreover, the pharmacokinetic properties of the lead compound **3h**, including aqueous solubility, blood-brain barrier penetration, CYP2D6 binding, hepatotoxicity, intestinal absorption, and plasma-protein binding, were calculated and predicted. The results of ADME analysis are presented in Figure 4. The biplot figure showed two analogous 95% and 99% confidence ellipses for the blood-brain barrier penetration and human intestinal absorption models, respectively. The detailed results of pharmacokinetic properties for derivative **3h** are shown in Table 4.

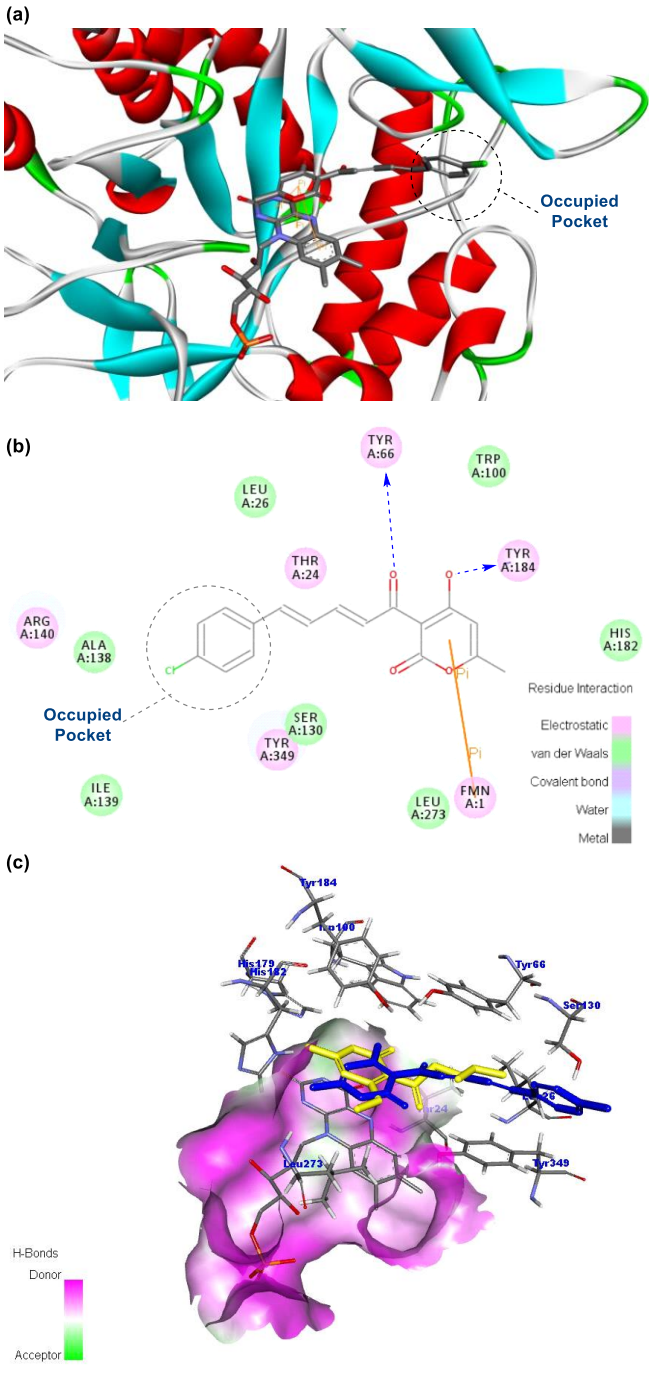

Fig. 3 Molecular docking of optimized derivative **3h** (ball-and-stick) and PETNR (space-filling). (a) 3D binding mode of compound **3h** and PETNR with π-π interaction. (b) 2D contour of the binding mode generated using the Accelrys Discovery Studio Package, including electrostatic interactions (pink), van der Waals forces (green) and H-bond interactions (blue arrow). (c) 3D binding mode of both Pogostone (yellow skeleton) and optimized compound **3h** (blue skeleton) with key amino acid residues of PETNR.

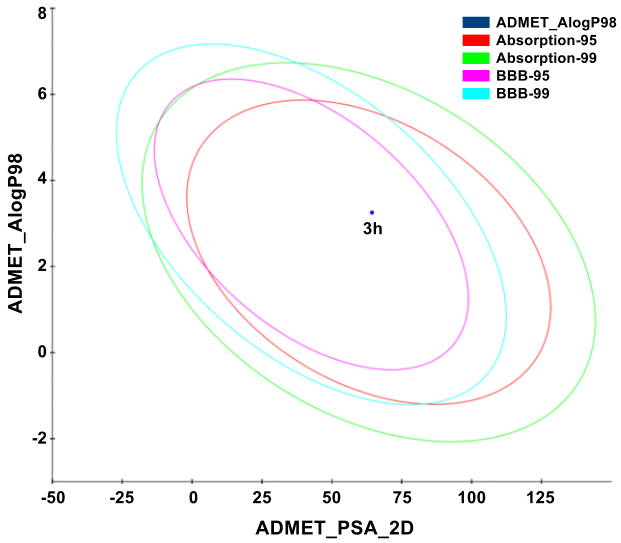

Fig. 4 Plot of PSA versus AlogP for compound **3h** showing the 95% and 99% confidence limit ellipses corresponding to the blood-brain barrier and intestinal absorption models. Abbreviations: ADMET, absorption, distribution, metabolism, excretion and toxicity; AlogP, the logarithm of the partition coefficient between n-octanol and water; BBB, blood-brain barrier; PSA, polar surface area; 2D, two-dimensional.

View Article Online
DOI: 10.1039/C7OB01429E

Table 3 Antibacterial activities *in vitro* [MIC (μg/mL)], and LibDock score of the Pogostone derivatives

PD	*E. coli* ATCC 25922	*E. coli* CMCC 44102	*S. aureus* ATCC 25923	*S. aureus* CMCC 26003	MRSA ATCC 43300	MRSA ATCC 33591	LibDock Score[a]
3a	>256	>256	64	128	64	64	105.082
3b	>512	>512	128	128	128	128	95.366
3c	>256	>256	128	128	128	128	97.340
3d	>512	>512	512	512	512	512	95.645
3e	>256	>256	256	256	256	256	95.481
3f	>256	>256	128	128	128	128	95.829
3g	>256	>265	64	64	64	64	108.725
3h	>256	>256	16	16	8	8	116.710
3i	>256	>265	64	64	64	64	105.408
3j	>512	>512	512	512	512	512	97.569
3k	>256	>256	>256	>256	>256	>256	94.404
3l	>256	>256	>256	>256	>256	>256	94.975
3m	>256	>256	>256	>256	>256	>256	94.889
3n	>256	>256	64	64	128	128	110.125
3o	>256	>256	64	64	64	64	101.992
Lev.	16	16	2	2	4	4	-
Van.	NT	NT	1	1	1	1	-

[a] Molecular docking studies were performed to generate the LibDock scores by using the LibDock module in DS software. Abbreviations: NT, not test; ATCC, American Type Culture Collection; CMCC, Center for Medical Culture Collection in China; PD, Pogostone Derivative; Lev., Levofloxacin; Van., Vancomycin

Table 4 ADMET prediction and pharmacokinetic properties of compound **3h**

Compound name	Aqueous solubility level	BBB penetration level	CYP2D6 binding prediction	Hepatotoxicity prediction	Intestinal absorption level	Plasma protein binding	PSA	AlogP98
3h	0 (insoluble)	2 (medium)	False (non-inhibitor)	False (nontoxic)	0 (good)	True (highly bounded)	64.347	3.254

Abbreviations: AlogP, the logarithm of the partition coefficient between n-octanol and water; PSA, polar surface area; ADMET, absorption, distribution, metabolism, excretion and toxicity.

Conclusions

Pogostone is a key antibacterial ingredient in the traditional Chinese medicine *Pogostemon cabli*. Here we generate a pharmacologically interesting library of Pogostone derivatives with diverse electronic and steric modifications based on rational design involving molecular docking and analysis of structure-activity relationships. The derivatives were prepared using a custom-designed, efficient, green organocatalytic reaction involving Knoevenagel condensation of the Pogostone core with α,β-unsaturated aldehyde. Several derivatives, especially **3h**, show promising antibacterial activity *in vitro* against *S. aureus* and MRSA. Further work is underway in our laboratory to modify the lead compound **3h** and to explore medicinal applications of this and other Pogostone derivatives.

Conflicts of interest

There are no conflicts of interest to declare.

Acknowledgements

We are grateful for financial support from the National Natural Science Foundation of China (81573588 and 81630101), the Science & Technology Department of Sichuan Province (2017JQ0002), the Foundation for the Author of National Excellent Doctoral Dissertation of PR China (201487) and the China Postdoctoral Science Foundation.

Experimental section

Molecular docking

Molecular docking was performed using the CDOCKER program embedded in the Accelrys Discovery Studio 3.5 package (DS 3.5). The Pogostone structure was generated by DS 3.5, and then

minimized using the CHARMM27 force field. The crystal structure of PETNR (scPDB: P71278) was used for docking. The binding site was defined to be the interaction residues Thr24, Leu26, Tyr66, Trp100, His182, Tyr184 and Tyr349; the radius was 10 Å. Automated molecular docking was performed using the "partial flexibility" CDOCKER tool in DS 3.5 in the presence of zinc cofactor. The best molecular docking results were identified based on docking scores and binding free energy. DS 3.5 was used to identify and visualize hydrogen bonds as well as hydrophobic, hydrophilic and coordination interactions with amino acid residues in the enzyme active site.

Chemistry

General information

NMR data were obtained for ^{1}H at 400 MHz and for ^{13}C at 100 MHz, or for ^{1}H at 600 MHz and for ^{13}C at 150 MHz. Chemical shifts were reported in parts per million (ppm) using tetramethylsilane as internal standard with solvent resonance in $CDCl_3$. Mass spectra were recorded using electrospray ionization on a Q-TOF instrument. Column chromatography was performed on a silica gel (200-300 mesh) using an eluent of ethyl acetate and petroleum ether. TLC was performed on glass-backed silica plates; products were visualized using UV light. Melting points were determined on a Mel-Temp apparatus.

General procedure for the synthesis of Pogostone derivatives 3

To dehydroacetic acid **1** (50.4 mg, 0.3 mmol), amine catalyst **C5** (35.9 mg, 0.06 mmol), benzoic acid (14.7 mg, 0.12 mmol) and MeCN (1.5 mL) in a standard glass vial with stir bar was added α,β-unsaturated aldehyde **2** (0.36 mmol in 0.5 mL MeCN). The reaction mixture was stirred at room temperature until the reaction was complete based on TLC. The reaction mixture was concentrated, and the residue was purified by flash chromatography on a silica gel (Petroleum ether / Ethyl Acetate = 7:1) to give the Pogostone derivatives **3,** which were dried under vacuum and further analyzed by ^{1}H NMR, ^{13}C NMR and high-resolution mass spectrometry.

4-hydroxy-6-methyl-3-((2*E*,4*E*)-5-phenylpenta-2,4-dieno-yl)-2*H*-pyran-2-one (3a): yellow solid, 72.6 mg, 84% yield, m.p. 168-172 °C. ^{1}H NMR (600 MHz, $CDCl_3$): δ = 7.84 (d, *J* = 15.0 Hz, 1H), 7.77 (dd, *J* = 15.0, 10.2 Hz, 1H), 7.51 (d, *J* = 7.2 Hz, 2H), 7.38 (t, *J* = 7.2 Hz, 2H), 7.34 (t, *J* = 6.6 Hz, 1H), 7.11 (dd, *J* = 15.6, 10.2 Hz, 1H), 7.05 (d, *J* = 15.6 Hz, 1H), 5.95 (s, 1H), 2.27 (s, 3H) ppm . ^{13}C NMR (100 MHz, $CDCl_3$): δ = 192.3, 183.4, 168.4, 161.2, 146.7, 143.4, 135.9, 129.6, 128.9, 127.6, 127.4, 126.3, 102.6, 99.3, 20.6 ppm. HRMS (ESI): *m/z* calculated for $C_{17}H_{14}O_4$+Na: 305.0790, found: 305.0792.

(1'*S*,2'*S*,3'*S*)-2'-(4-hydroxy-6-methyl-2-oxo-2*H*-pyran-3-carbonyl)-1',2',3',6'-tetrahydro-[1,1':3',1''-terphenyl]-4'-carbaldehyde (4a): white solid, 11.2 mg, 19% yield, m.p. 121-124 °C, ^{1}H NMR (400 MHz, $CDCl_3$): δ = 9.52 (s, 1H), 7.41 (d, *J* = 7.2 Hz, 2H), 7.30 (t, *J* = 7.6 Hz, 2H), 7.18 (dd, *J* = 15.2, 7.2 Hz, 4H), 7.08 (d, *J* = 7.2 Hz, 2H), 5.86 (s, 1H), 4.79 (s, 1H), 4.26 (s, 1H), 3.37-3.31 (m, 2H), 3.01-2.95 (m, 1H), 2.22 (s, 3H) ppm. ^{13}C NMR (100 MHz, $CDCl_3$): δ = 207.6, 192.7, 181.7, 169.1, 160.8, 152.8, 141.5, 141.3, 139.9, 128.6, 128.4, 128.3, 127.6, 126.8, 126.7, 101.7, 99.7, 53.0, 40.0, 36.7, 31.1, 20.6 ppm. HRMS (ESI): *m/z* calculated for $C_{26}H_{22}O_5$+Na: 437.1365, found: 437.1364.

3-((2*E*,4*E*)-5-(2-fluoro-phenyl)penta-2,4-dieno-yl)-4-hydroxy-6-methyl-2*H*-pyran-2-one (3b): yellow solid, 72.9 mg, 79% yield, m.p. 189-192 °C. ^{1}H NMR (400 MHz, $CDCl_3$): δ = 7.86 (d, *J* = 15.2 Hz, 1H), 7.75 (dd, *J* = 14.8, 9.2 Hz, 1H), 7.57 (t, *J* = 7.6 Hz, 1H), 7.34-7.28 (m, 1H), 7.19-7.06 (m, 4H), 5.95 (s, 1H), 2.27 (s, 3H) ppm. ^{13}C NMR (100 MHz, $CDCl_3$): δ = 192.4, 183.3, 168.5, 161.2, 160.9 (d, J_{CF} = 251.3 Hz), 146.5, 135.3 (d, J_{CF} = 3.3 Hz), 130.9 (d, J_{CF} = 8.6 Hz), 129.6 (d, J_{CF} = 5.6 Hz), 127.9 (d, J_{CF} = 3.0 Hz), 127.1, 124.4 (d, J_{CF} = 3.5 Hz), 124.0 (d, J_{CF} = 11.7 Hz), 116.1 (d, J_{CF} = 21.9 Hz), 102.5, 99.4, 20.6 ppm. HRMS (ESI): *m/z* calculated for $C_{17}H_{13}FO_4$+Na: 323.0696, found: 323.0700.

3-((2*E*,4*E*)-5-(2-chloro-phenyl)penta-2,4-dieno-yl)-4-hydroxy-6-methyl-2*H*-pyran-2-one (3c): yellow solid, 74.6 mg, 77% yield, m.p. 154-156 °C. ^{1}H NMR (400 MHz, $CDCl_3$): δ = 7.87 (d, *J* = 14.8 Hz, 1H), 7.79 (dd, *J* = 15.2, 10.8 Hz, 1H), 7.68 (dd, *J* = 7.6, 2.4 Hz, 1H), 7.47 (d, *J* = 15.6 Hz, 1H), 7.40 (dd, *J* = 7.6, 2.0 Hz, 1H), 7.31-7.24 (m, 2H), 7.08 (dd, *J* = 15.6, 10.4Hz, 1H), 5.95 (s, 1H), 2.27 (s, 3H) ppm. ^{13}C NMR (100 MHz, $CDCl_3$): δ = 192.3, 183.3, 168.6, 161.2, 146.1, 138.5, 134.4, 133.9, 130.3, 130.1, 129.5, 127.4, 127.1, 127.0, 102.5, 99.4, 20.6 ppm. HRMS (ESI): *m/z* calculated for $C_{17}H_{13}ClO_4$+Na: 339.0400, found: 339.0397.

4-hydroxy-6-methyl-3-((2*E*,4*E*)-5-(2-nitrophenyl)penta-2,4-dienoyl)-2*H*-pyran-2-one (3d): yellow solid, 78.4 mg, 78% yield, m.p. 193-196 °C. ^{1}H NMR (400 MHz, $CDCl_3$): δ = 8.00 (d, *J* = 8.0 Hz, 1H), 7.90 (d, *J* = 14.8 Hz, 1H), 7.78-7.71 (m, 2H), 7.64 (t, *J* = 7.6 Hz, 1H), 7.55-7.47 (m, 2H), 7.06 (dd, *J* = 15.6, 11.2 Hz, 1H), 5.97 (s, 1H), 2.29 (s, 3H) ppm. ^{13}C NMR (100 MHz, $CDCl_3$): δ = 192.4, 183.1, 168.8, 161.2, 148.1, 145.0, 136.8, 133.3, 132.0, 131.5, 129.5, 128.8, 128.4, 125.0, 102.4, 99.5, 20.7 ppm. HRMS (ESI): *m/z* calculated for $C_{17}H_{13}NO_6$+Na: 350.0641, found: 350.0638.

3-((2*E*,4*E*)-5-(3-fluorophenyl)penta-2,4-dienoyl)-4-hydroxy-6-methyl-2*H*-pyran-2-one (3f): yellow solid, 73.8 mg, 80% yield, m.p. 199-202 °C. ^{1}H NMR (400 MHz, $CDCl_3$): δ = 7.86 (d, *J* = 15.2 Hz, 1H), 7.73 (dd, *J* = 15.2, 10.4 Hz, 1H), 7.37-7.27 (m, 2H), 7.20 (d, *J* = 10.0 Hz, 1H), 7.09 (dd, *J* = 15.6, 10.4 Hz, 1H), 7.04 (d, *J* = 8.4 Hz, 1H), 7.00 (d, *J* = 15.6 Hz, 1H), 5.96 (s, 1H), 2.28 (s, 3H) ppm. ^{13}C NMR (100 MHz, $CDCl_3$): δ = 192.4, 183.3, 168.6, 163.1 (d, J_{CF} = 245.0 Hz), 161.2, 145.8, 141.6 (d, J_{CF} = 2.8 Hz), 138.2 (d, J_{CF} = 7.6 Hz), 130.4 (d, J_{CF} = 8.3 Hz), 128.6, 127.3, 123.4 (d, J_{CF} = 2.8 Hz), 116.3 (d, J_{CF} = 21.3 Hz), 113.8 (d, J_{CF} = 21.9 Hz), 102.5, 99.4, 20.7 ppm. HRMS (ESI): *m/z* calculated for $C_{17}H_{13}FO_4$+Na: 323.0696, found: 323.0698.

3-((2*E*,4*E*)-5-(3-chlorophenyl)penta-2,4-dienoyl)-4-hydroxy-6-methyl-2*H*-pyran-2-one (3f): yellow solid, 76.8 mg, 79% yield, m.p. 165-168 °C. ^{1}H NMR (400 MHz, $CDCl_3$): δ = 7.86 (d, *J* = 14.8 Hz, 1H), 7.71 (dd, *J* = 14.8, 10.8 Hz, 1H), 7.48 (s, 1H), 7.38-7.29 (m, 3H), 7.09 (dd, *J* = 15.2, 10.8 Hz, 1H), 6.96 (d, *J* = 15.6 Hz, 1H),

View Article Online
DOI: 10.1039/C7OB01420E

5.95 (s, 1H), 2.27 (s, 3H) ppm. ^{13}C NMR (100 MHz, $CDCl_3$): δ = 192.3, 183.3, 168.6, 161.2, 145.7, 141.3, 137.8, 134.9, 130.1, 129.3, 128.7, 127.4, 127.4, 125.6, 102.5, 99.4, 20.6 ppm. HRMS (ESI): *m/z* calculated for $C_{17}H_{13}ClO_4$+Na: 339.0400, found: 339.0401.

3-((2*E*,4*E*)-5-(4-fluorophenyl)penta-2,4-dienoyl)-4-hydroxy-6-methyl-2*H*-pyran-2-one (3g): yellow solid, 75.6 mg, 82% yield, m.p. 189-192 °C. ^{1}H NMR (400 MHz, $CDCl_3$): δ = 7.85-7.70 (m, 2H), 7.50-7.47 (m, 2H), 7.08-7.00 (m, 4H), 5.94 (s, 1H), 2.27 (s, 3H) ppm. ^{13}C NMR (100 MHz, $CDCl_3$): δ = 192.3, 183.3, 168.5, 163.4 (d, J_{CF} = 249.3 Hz), 161.2, 146.4, 141.9 (d, J_{CF} = 0.9 Hz), 132.2 (d, J_{CF} = 3.4 Hz), 129.3 (d, J_{CF} = 8.2 Hz), 127.2 (d, J_{CF} = 2.4 Hz), 126.4 (d, J_{CF} = 0.8 Hz), 116.0 (d, J_{CF} = 21.8 Hz), 102.6, 99.3, 20.6 ppm. HRMS (ESI): *m/z* calculated for $C_{17}H_{13}FO_4$+Na: 323.0696, found: 323.0701.

3-((2*E*,4*E*)-5-(4-chlorophenyl)penta-2,4-dienoyl)-4-hydroxy-6-methyl-2*H*-pyran-2-one (3h): yellow solid, 82.8 mg, 85% yield, m.p. 174-176 °C. ^{1}H NMR (400 MHz, $CDCl_3$): δ = 7.84 (d, *J* = 15.2 Hz, 1H), 7.72 (dd, *J* = 15.2, 10.4 Hz, 1H), 7.43 (d, *J* = 8.4 Hz, 2H), 7.34 (d, *J* = 8.4 Hz, 2H), 7.06 (dd, *J* = 15.6, 10.4 Hz, 1H), 6.98 (d, *J* = 15.2 Hz, 1H), 5.95 (s, 1H), 2.27 (s, 3H) ppm. ^{13}C NMR (100 MHz, $CDCl_3$): δ = 192.3, 183.3, 168.5, 161.2, 146.1, 141.6, 135.3, 134.5, 129.2, 128.7, 127.9, 126.9, 102.5, 99.4, 20.6 ppm. HRMS (ESI): *m/z* calculated for $C_{17}H_{13}ClO_4$+Na: 339.0400, found: 339.0399.

3-((2*E*,4*E*)-5-(4-bromophenyl)penta-2,4-dienoyl)-4-hydroxy-6-methyl-2*H*-pyran-2-one (3i): yellow solid, 92.1 mg, 83% yield, m.p. 179-182 °C. ^{1}H NMR (400 MHz, $CDCl_3$): δ = 7.84 (d, *J* = 15.2 Hz, 1H), 7.71 (dd, *J* = 15.2, 10.2 Hz, 1H), 7.50 (d, *J* = 8.4 Hz, 2H), 7.36 (d, *J* = 8.4 Hz, 2H), 7.07 (dd, *J* = 15.6, 10.8 Hz, 1H), 6.96 (d, *J* = 15.2 Hz, 1H), 5.94 (s, 1H), 2.27 (s, 3H) ppm. ^{13}C NMR (100 MHz, $CDCl_3$): δ = 192.3, 183.3, 168.5, 161.2, 146.1, 141.7, 134.9, 132.1, 128.9, 128.0, 127.0, 123.6, 102.5, 99.4, 20.6 ppm. HRMS (ESI): *m/z* calculated for $C_{17}H_{13}BrO_4$+Na: 382.9895, found: 382.9893.

4-hydroxy-6-methyl-3-((2*E*,4*E*)-5-(*p*-tolyl)penta-2,4-dienoyl)-2*H*-pyran-2-one (3j): yellow solid, 66.4 mg, 72% yield, m.p. 180-182 °C. ^{1}H NMR (400 MHz, $CDCl_3$): δ = 7.81 (d, *J* = 14.4 Hz, 1H), 7.75 (dd, *J* = 14.4, 8.8 Hz, 1H), 7.40 (d, *J* = 8.0 Hz, 2H), 7.18 (d, *J* = 7.6 Hz, 2H), 7.09-6.99 (m, 2H), 5.92 (s, 1H), 2.36 (s, 3H), 2.25 (s, 3H) ppm. ^{13}C NMR (100 MHz, $CDCl_3$): δ = 192.2, 183.4, 168.3, 161.2, 147.2, 143.7, 140.0, 133.3, 129.7, 127.6, 126.5, 125.7, 102.6, 99.3, 21.3, 20.6 ppm. HRMS (ESI): *m/z* calculated for $C_{18}H_{16}O_4$+Na: 319.0946, found: 319.0941.

4-hydroxy-3-((2*E*,4*E*)-5-(2-methoxyphenyl)penta-2,4-dienoyl)-6-methyl-2*H*-pyran-2-one (3k): yellow solid, 70.1 mg, 73% yield, m.p. 153-155 °C. ^{1}H NMR (400 MHz, $CDCl_3$): δ = 7.80 (d, *J* = 2.0 Hz, 1H), 7.79 (s, 1H), 7.53 (dd, *J* = 8.0, 1.6 Hz, 1H), 7.40 (d, *J* = 15.6 Hz, 1H), 7.30 (t, *J* = 7.6 Hz, 1H), 7.20-7.13 (m, 1H), 6.96 (t, *J* = 7.6 Hz, 1H), 6.90 (d, *J* = 8.4 Hz, 1H), 5.92 (s, 1H), 3.89 (s, 3H), 2.25 (s, 3H) ppm. ^{13}C NMR (100 MHz, $CDCl_3$): δ = 192.2, 183.5, 168.2, 161.3, 157.8, 148.2, 139.0, 130.9, 128.1, 128.0, 125.4, 124.9, 120.8, 111.1, 102.7, 99.3, 55.5, 20.6 ppm. HRMS (ESI): *m/z* calculated for $C_{18}H_{16}O_5$+Na: 335.0895, found: 335.0897.

4-hydroxy-3-((2*E*,4*E*)-5-(4-methoxyphenyl)penta-2,4-dienoyl)-6-methyl-2*H*-pyran-2-one (3l): yellow solid, 71.7 mg, 75% yield, m.p. 152-155 °C. ^{1}H NMR (400 MHz, $CDCl_3$): δ = 7.80-7.72 (m, 2H), 7.45 (d, *J* = 8.8 Hz, 2H), 7.03-6.93 (m, 2H), 6.90 (d, *J* = 8.8 Hz, 2H), 5.92 (s, 1H), 3.84 (s, 3H), 2.25 (s, 3H) ppm. ^{13}C NMR (100 MHz, $CDCl_3$): δ = 192.0, 183.5, 168.1, 161.3, 161.0, 147.5, 143.5, 129.3, 128.8, 125.4, 125.0, 114.4, 114.4, 102.7, 99.2, 55.4, 20.6 ppm. HRMS (ESI): *m/z* calculated for $C_{18}H_{16}O_5$+Na: 335.0895, found: 335.0894.

3-((2*E*,4*E*)-5-(furan-2-yl)penta-2,4-dienoyl)-4-hydroxy-6-methyl-2*H*-pyran-2-one (3m): yellow solid, 59.5 mg, 71% yield, m.p. 178-181 °C. ^{1}H NMR (400 MHz, $CDCl_3$): δ = 7.82 (d, *J* = 14.8 Hz, 1H), 7.70 (dd, *J* = 15.2, 11.2 Hz, 1H), 7.48 (d, *J* = 1.2 Hz, 1H), 6.98 (dd, *J* = 15.2, 11.2 Hz, 1H), 6.81 (d, *J* = 15.6 Hz, 1H), 6.54 (d, *J* = 3.2 Hz, 1H), 6.47 (q, *J* = 1.6 Hz, 1H), 5.93 (s, 1H), 2.26 (s, 3H) ppm. ^{13}C NMR (100 MHz, $CDCl_3$): δ = 192.0, 183.4, 168.3, 161.2, 152.3, 146.3, 144.4, 129.5, 126.1, 125.8, 113.2, 112.5, 102.6, 99.3, 20.6 ppm. HRMS (ESI): *m/z* calculated for $C_{15}H_{12}O_5$+Na: 295.0582, found: 295.0580.

4-hydroxy-6-methyl-3-((2*E*,4*E*)-6-methylhepta-2,4-dieno-yl)-2H-pyran-2-one (3o): pale yellow, 36.7 mg, 48% yield, m.p. 79-81 °C. ^{1}H NMR (400 MHz, $CDCl_3$): δ = 5.91 (s, 1H), 5.47 (dd, *J* = 15.6, 6.8 Hz, 1H), 5.29 (dd, *J* = 15.6, 8.8 Hz, 1H), 4.36 (dd, *J* = 10.4, 6.8 Hz, 1H), 4.19 (dd, *J* = 17.6, 8.4 Hz, 1H), 2.25 (s, 3H), 2.11 (dq, *J* = 13.6, 6.8 Hz, 1H), 0.79 (dd, *J* = 12.4, 6.8 Hz, 6H) ppm. ^{13}C NMR (100 MHz, $CDCl_3$): δ = 205.5, 180.6, 168.9, 160.4, 140.9, 124.4, 101.3, 100.2, 51.1, 37.3, 30.8, 22.4, 22.3, 20.7 ppm. HRMS (ESI): *m/z* calculated for $C_{14}H_{16}O_4$+Na: 271.0946, found: 271.0948.

3-((2E,4E)-hexa-2,4-dienoyl)-4-hydroxy-6-methyl-2H-pyran-2-one (3o): yellow solid, 29.3 mg, 43% yield, *Z*/*E* ratio 2.5:1, m.p. 85-87 °C. ^{1}H NMR (400 MHz, $CDCl_3$): δ = 7.72-7.53 (m, 2H), 6.51-6.29 (m, 2H), 5.92 (s, 1H), 2.26 (s, 3H), 1.92 (d, *J* = 6.0 Hz, 2H), 1.84 (d, *J* = 6.8 Hz, 1H). ^{13}C NMR (100 MHz, $CDCl_3$): δ = 192.9, 183.3, 168.3, 161.2, 147.2, 143.1, 131.2, 124.2, 102.5, 99.2, 20.6, 19.1 ppm. HRMS (ESI): *m/z* calculated for $C_{12}H_{12}O_4$+Na: 243.0633, found: 243.0634.

Biological investigations

Bacteria

E. coli ATCC 25922, *E. coli* CMCC 44101, *S. aureus* ATCC 25923, *S. aureus* CMCC 26003, MRSA ATCC 43300 and MRSA ATCC 33591 were cultured in trypticase soy broth at 37 °C.

***In vitro* MIC assay**

The MIC of each compound was determined using a standard broth microdilution assay[21] consistent with the guidelines of the Clinical Laboratory Standards Institute. Stock solutions of test compounds were diluted in a 2-fold series to achieve the desired concentrations. The MIC was defined as the lowest concentration of the chemical that inhibited the development of visible bacterial growth after incubation at 37 °C for 18-24 h.

Notes and references

1 For recent reviews on antibiotics, see: (*a*) M. Ferrer, C. Méndez-García, D. Rojo, C. Barbas and A. Moya, *Biochem. Pharmacol.*, 2017, **134**, 114-126; (*b*) S. R. Modi, J. J. Collins and D. A. Relman, *J. Clin. Invest.*, 2014, **124**, 4212-4218; (*c*) J. Bérdy, *J. Antibiot.*, 2005, **58**, 1-26; (*d*) A. L. Demain and S. Sanchez, *J. Antibiot.*, 2009, **62**, 5-16.

2 For recent reviews on resistance of antibiotics, see: (*a*) C. A. Arias and B. E. Murray, *New Engl. J. Med.*, 2009, **360**, 439-443; (*b*) L. B. Rice, *Am. J. Infect. Control*, 2006, **34**, S11-S19; (*c*) F. Baquero, C. Alvarez-Ortega and J. L. Martinez, *Environ. Microbiol. Rep.*, 2009, **1**, 469-476; (*d*) J. Davies and D. Davies, *Microbiol. Mol. Biol. Rev.*, 2010, **74**, 417-433.

3 For recent reviews on the synthesis of antibacterial agents, see: (*a*) M. A. Farha and E. D. Brown, *Nat. Prod. Rep.*, 2016, **33**, 668-680; (*b*) K. P. Miller, L. Wang, B. C. Benicewicz and A. W. Decho, *Chem. Soc. Rev.*, 2015, **44**, 7787-7807; (*c*) Q.-F Zheng, H. Fang and W. Liu, *Org. Biomol. Chem.*, 2017, **15**, 3376-3390; (d) G. Devasahayam, W. M. Scheld and P. S. Hoffman, *Expert Opin. Inv. Drugs*, 2010, **19**, 215-234.

4 For selected examples of antibacterial agents, see: (*a*) W. He, B. M. Griffiths, W. Wang and X. Wang, *Org. Biomol. Chem.*, 2017, **15**, 4241-4245; (*b*) A. Vermote, G. Brackman, M. D. P. Risseeuw, B. Vanhoutte, P. Cos, K. Van Hecke, K. Breyne, E. Meyer, T. Coenye and S. Van Calenbergh, *Angew. Chem. Int. Ed.*, 2016, **55**, 6551-6555; (*c*) P. Teng, D. Huo, A. Nimmagadda, J.-F. Wu, F.-Y. She, M. Su, X.-Y. Lin, J.-Y. Yan, A.-N. Cao, C.-W. Xi, Y. Hu and J.-F. Cai, *J. Med. Chem.*, 2016, **59**, 7877-7887; (*d*) P. Panchaud, T. Bruyère, A. C. Blumstein, D. Bur, A. Chambovey, E. A. Ertel, M. Gude, C. Hubschwerlen, L. Jacob, T. Kimmerlin, T. Pfeifer, L. Prade, P. Seiler, D. Ritz and G. Rueedi, *J. Med. Chem.*, 2017, **60**, 3755-3775; (*e*) S. R. Mandha, S. Siliveri, M. Alla, V. R. Bommena, M. R. Bommineni and S. Balasubramanian, *Bioorg. Med. Chem. Lett.*, 2012, **22**, 5272-5278; (*f*) M. Kidwai, S. Saxena, M. K. Rahman Khan and S. S. Thukral, *Bioorg. Med. Chem. Lett.*, 2005, **15**, 4295-4298.

5 (*a*) A. L. Harvey, *Drug Discov. Today*, 2008, **13**, 894-901; (*b*) D. G. Brown, T. Lister and T. L. May-Dracka, *Bioorg. Med. Chem. Lett.*, 2014, **24**, 413-418; (*c*) D. J. Newman and G. M. Cragg, *J. Nat. Prod.*, 2012, **75**, 311-335.

6 (*a*) G. Karageorgis, S. Warriner and A. Nelson, *Nat. Chem.*, 2014, **6**, 872-876; (*b*) T. Rodrigues, D. Reker, P. Schneider and G. Schneider, *Nat. Chem.*, 2016, **8**, 531-541; (*c*) K. Kumar and H. Waldmann, *Angew. Chem. Int. Ed.*, 2009, **48**, 3224-3242.

7 (*a*) R. Narayan, J. O. Bauer, C. Strohmann, A. P. Antonchick and H. Waldmann, *Angew. Chem. Int. Ed.*, 2013, **52**, 12892-12896; (*b*) T. J. Zimmermann, S. Roy, N. E. Martinez, S. Ziegler, C. Hedberg and H. Waldmann, *ChemBioChem*, 2013, **14**, 295-300; (*c*) J. Richers, A. Pöthig, E. Herdtweck, C. Sippel, F. Hausch and K. Tiefenbacher, *Chem.-Eur. J.*, 2017, **23**, 3178-3183; (*d*) P. K. Chinthakindi, J. Singh, S. Gupta, A. Nargotra, P. Mahajan, A. Kaul, Z. Ahmed, S. Koul and P. L. Sangwan, *Eur. J. Med. Chem.*, 2017, **127**, 1047-1058; (*e*) S.-P. Wu, L.-L. Yang, W.-J. Sun, L.-L. Si, S.-L. Xiao, Q. Wang, L. Dechoux, S. Thorimbert, M. Sollogoub, D. M. Zhou and Y. M. Zhang, *Eur. J. Med. Chem.*, 2017, **130**, 308-319; (*f*) Z.-P. Xiong, J.-F. Niu, H. Liu, Z.-H. Xu, J.-K. Li and Q.-L. Wu, *Bioorg. Med. Chem. Lett.*, 2017, **27**, 2010-2013; (*g*) B. Liang, S.-J. Yu, J. Li, F. Wang, G.-L. Liang, A. Zhang and C.-Y. Ding, *Tetrahedron Lett.*, 2017, **58**, 1822-1825; (*h*) P. A. Yadav, C. P. Kumar, B. Siva, K. S. Babu, A. D. Allanki, P. S. Sijwali, N. Jain and A. V. Rao, *Eur. J. Med. Chem.*, 2017, **134**, 242-257.

8 E. I. Parkinson, J. S. Bair, B. A. Nakamura, H. Y. Lee, H. I. Kuttab, E. H. Southgate, S. Lezmi, G. W. Lau and P. J. Hergenrother, *Nat. Commun.*, 2015, **6**, article number: 6947.

9 (*a*) Z.-B. Zhang, X.-Y. Chen, H.-B. Chen, L. Wang, J.-L. Liang, D.-D. Luo, Y.-H. Liu, H.-M. Yang, Y.-C. Li, J.-H. Xie and Z.-R. Su, *Eur. J. Pharmacol.*, 2016, **781**, 229-238; (*b*) H. Chen, H. Liao, Y. Liu, Y. Zheng, X. Wu, Z. Su, X. Zhang, Z. Lai, X. Lai and Z. X. Lin, *Fitoterapia*, 2015, **100**, 110–117; (*c*) X. Yang, X. Zhang, S.-P. Yang and W.-Q. Liu, *Iran. J. Pharm. Res.*, 2013, **12**, 307-316; (*d*) T.-C. Lu, J.-C. Liao, T.-H. Huang, Y.-C. Lin, C.-Y. Liu, Y.-J. Chiu and W.-H. Peng, *Evid. Based Compl. Alternat. Med.*, 2011, article ID: 671741.

10 (*a*) A. Paul, S. Bakshi, D. P. Sahoo, M. C. Kalita and L. Sahoo, *Appl. Biochem. Biotechnol.*, 2012, **166**, 1871-1895; (*b*) D. Kocevski, M. Du, J.-Q. Kan, C.-J. Jing, I. Lačanin and H. Pavlović, *J. Food Sci.*, 2013, **78**, M731-M737.

11 F. Peng, F. Wan, L. Xiong, C. Peng, M. Dai and J. Chen, *Chinese Med. J.*, 2014, **127**, 4001-4005.

12 (*a*) R.-Q. Zhang, P.-A. Yan, Y.-X. Li, L. Xiong, X.-H. Gong and C. Peng, *Eur. J. Drug Metab. Pharmacokinet.*, 2016, **41**, 441-448; (*b*) Y.-C. Li, H.-C. Liang, H.-M. Chen, L.-R. Tan, Y.-Y. Yi, Z. Qin, W.-M. Zhang, D.-W. Wu, C.-W. Li, R.-F. Lin, Z.-R. Su and X.-P. Lai, *Phytomedicine*, 2012, **20**, 77-83.

13 Z.-W. Tang, X. Xie, W. Huang, H.-J. Leng, B. Wang, B. Han and C. Peng, *Lat. Am. J. Pharm.*, 2016, **35**, 502-509.

14 (*a*) C. R. Pudney, S. Hay and N. S. Scrutton, *FEBS J.*, 2009, **276**, 4780-4789; (*b*) C. R. Pudney, S. Hay, C. Levy, J. Y. Pang, M. J. Sutcliffe, D. Leys and N. S. Scrutton, *J. Am. Chem. Soc.*, 2009, **131**, 17072-17073; (*c*) C. A. Haynes, R. L. Koder, A. F. Miller and D. W. Rodgers, *J. Biol. Chem.*, 2002, **277**, 11513-11520.

15 A. A. Fadda and K. M. Elattar, *Synth. Commun.*, 2016, **46**, 1-30.

16 Y.-Y. Yi, J.-J. He, J.-Q. Su, S.-Z. Kong, J.-Y. Su, Y.-C. Li, S.-H. Huang, C.-W. Li, X.-P. Lai and Z.-R. Su, *Fitoterapia*, 2013, **84**, 135-139.

17 (*a*) X. Li, W. Huang, Y.-Q. Liu, J.-W. Kang, D. Xia, G. He, C. Peng and B. Han, *J. Org. Chem.*, 2017, **82**, 397-406; (*b*) J.-L. Li, K.-C. Yang, Y. Li, Q. Li, H.-P. Zhu, B. Han, C. Peng, Y.-G. Zhi and X.-J. Gou, *Chem. Commun.*, 2016, **52**, 10617-10620; (*c*) L. Yang, W. Huang, X.-H. He, M.-C. Yang, X. Li, G. He, C. Peng and B. Han, *Adv. Synth. Catal.*, 2016, **358**, 2970-2975; (*d*) X.-H. He, L. Yang, W. Huang, Q. Zhao, X.-L. Pan, D.-F. Jiang, M.-C. Yang, C. Peng and B. Han, *RSC Adv.*, 2016, **6**, 28960-28965; (*e*) R. Zhou, Q. J. Wu, M.-R. Guo, W. Huang, X.-H. He, L. Yang, F. Peng, G. He and B. Han, *Chem. Commun.*, 2015, **51**, 13113-13116; (*f*) B. Han, W. Huang, W. Ren, G. He, J.-H. Wang and C. Peng, *Adv. Synth. Catal.*, 2015, **357**, 561-568; (*g*) Q. Zhao, B. Han, B. Wang, H.-J. Leng, C. Peng and W. Huang, *RSC Adv.*, 2015, **5**, 26972-26976; (*h*) B. Wang, H.-J. Leng, X.-Y. Yang, B. Han, C.-L. Rao, L. Liu, C. Peng and W. Huang, *RSC Adv.*, 2015, **5**, 88272-88276; (*i*) H.-J. Leng, F. Peng, S. Zingales, W. Huang, B. Wang, Q. Zhao, R. Zhou, G. He, C. Peng and B. Han, *Chem.-Eur. J.*, 2015, **21**, 18100-18108; (*j*) X. Li, L. Yang, C. Peng, X. Xie, H.-J. Leng, B. Wang, Z. W. Tang, G. He, L. Ouyang, W. Huang and B. Han, *Chem. Commun.*, 2013, **49**, 8692-8694; (*k*) X. Xie, C. Peng, G. He, H.-J. Leng, B. Wang, W. Huang and B. Han, *Chem. Commun.*, 2012, **48**, 10487-10489; (*l*) B. Han, Y.-C. Xiao, Y. Yao and Y.-C. Chen, *Angew. Chem. Int. Ed.*, 2010, **49**, 10189-10191.

18 For recent reviews on the organocatalysis in the medicinal chemistry, see: (*a*) P. A. Magriotis, *Eur. J. Org. Chem.*, 2014, **2014**, 2647-2657; (*b*) Y.-R. Wang, J.-J. Pan, Z.-D. Chen, X.-Q. Sun and Z.-M. Wang, *Mini-Rev. Med. Chem.*, 2013, **13**, 836-844; (*c*) J. Alemán and S. Cabrera, *Chem. Soc. Rev.*, 2013, **42**, 774-793.

19 CCDC 1555526 (**3a**) contains the supplementary crystallographic data for this paper. These data can be obtained free of charge from The Cambridge Crystallographic Data Centre via www.ccdc.cam.ac.uk/data_request/cif.

20 (*a*) C. Opoku-Temeng, N. Dayal, J. Miller and H. O. Sintim, *RSC Adv.*, 2017, **7**, 8288-8294; (*b*) M. M. Sallam, K. Abou-Aisha and M. El-Azizi, *Infect. Drug Resistance*, 2016, **9**, 301-311; (*c*) S. M. Wales, K. A. Hammer, A. M. King, A. J. Tague, D. Lyras, T. V. Riley, P. A. Keller and S. G. Pyne, *Org. Biomol. Chem.*, 2015, **13**, 5743-5756; (*d*) J. Li, C.-W. Lv, X.-J. Li, D. Qu, Z. Hou, M. Jia, X.-

View Article Online
DOI: 10.1039/C7OB01429E

X. Luo, X. Li and M.-K. Li, *Molecules*, 2015, **20**, 17469-17482; (*e*) J. Li, Z. Hou, G.-H. Chen, F. Li, Y. Zhou, X.-Y. Xue, Z.-P. Li, M. Jia, Z.-D. Zhang, M.-K. Li and X.-X. Luo, *Org. Biomol. Chem.*, 2014, **12**, 5528-5535.

21 (*a*) K.-C. Yang, J.-L. Li, X.-D. Shen, Q. Li, H.-J. Leng, Q. Huang, P.-K. Zheng, X.-J. Gou and Y.-G. Zhi, *RSC Adv.*, 2017, **7**, 21175-21179; (*b*) Y.-F. Li, H.-W. Sun, R. Gao, K.-Y. Liu, H.-Q. Zhang, Q.-H. Fu, S.-L. Qing, G. Guo and Q.-M. Zou, *Int. J. Nanomed.*, 2015, **10**, 447-462.

View Article Online
DOI: 10.1039/C7OB01429E

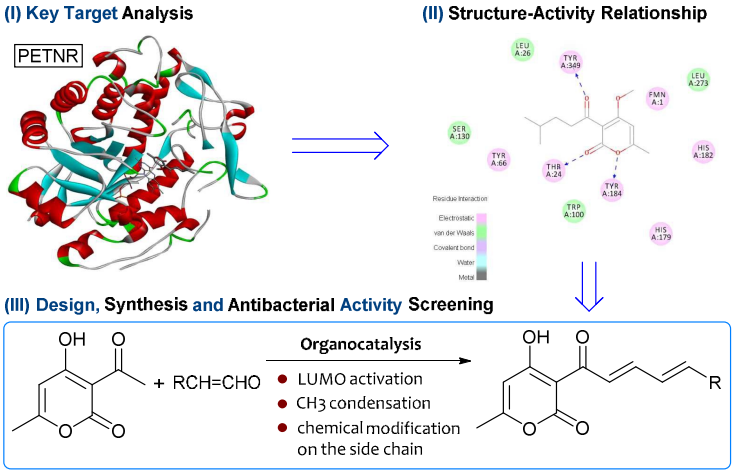

We performed molecular docking studies of Pogostone with PETNR and analyzed structure-activity relationships, which guided the structure design and the subsequent facile organocatalytic synthesis of Pogostone derivatives. Several of the synthesized compounds showed antibacterial activity *in vitro*, including one compound (**3h**) that was highly effective against MRSA.